JVI Accepted Manuscript Posted Online 19 December 2018 J. Virol. doi:10.1128/JVI.01952-18 Copyright © 2018 American Society for Microbiology. All Rights Reserved.

- Comparative analysis of gammaherpesvirus circRNA repertoires: conserved and unique viral
- 2 circRNAs.
- 3
- *Nathan Ungerleider¹, *Vaibhav Jain², *Yiping Wang³, Nicholas J Maness⁴, Robert V Blair⁵, Xavier Alvarez⁵, 4
- Cecily Midkiff⁵, Dennis Kolson⁶, Shanshan Bai⁷, Claire Roberts¹, Walter N Moss⁸, Xia Wang¹, Jacqueline 5
- Serfecz³, Michael Seddon⁹, Terri Lehman⁹, Tianfang Ma⁷, Yan Dong⁷, Rolf Renne², *Scott A Tibbetts³, and 6
- 7 *Erik K Flemington¹

8

- ¹Department of Pathology, Tulane University School of Medicine, Tulane Cancer Center, New Orleans, LA 9
- 10
- 11 ²Department of Biochemistry and Molecular Biology, University of Florida College of Medicine, Gainesville, FL
- 12
- 13 ³Department of Molecular Genetics and Microbiology, University of Florida, Gainesville, FL, 32610
- 14 ⁴Department of Microbiology and Immunology, Tulane Regional Primate Center, Covington, LA 70433
- ⁵Division of Comparative Pathology, Tulane Regional Primate Center, Covington, LA 70433 15
- 16 ⁶Department of Neurology, The Perelman School of Medicine, University of Pennsylvania, Philadelphia, PA

Downloaded from http://jvi.asm.org/ on January 4, 2019 by guest

- 17 19104
- 18 ⁷Department of Structural and Cellular Biology, Tulane University School of Medicine, Tulane Cancer Center,
- 19 New Orleans, LA 70112
- 20 ⁸Roy J. Carver Department of Biochemistry, Biophysics and Molecular Biology, Iowa State University, IA 50011
- ⁹Reprocell USA, Beltsville, MD 20705 21

22

- 23 *These authors contributed equally to this project.
- *Corresponding authors: Scott A Tibbetts (stibbe@ufl.edu), and Erik K Flemington (erik@tulane.edu) 24

25

- **KEYWORDS** 26
- 27 circRNA, circular RNA, circRPMS1_E4_E3a, circRPMS1_E4_E2, circEBNA_U, circvIRF4, circM11_ORF69,
- 28 non-coding RNA, lymphocryptovirus, rhadinovirus, Epstein Barr virus, EBV, Kaposi's sarcoma
- herpesvirus, KSHV, murid herpesvirus 68, MHV68, OriLyt 29

Downloaded from http://jvi.asm.org/ on January 4, 2019 by guest

ABSTRACT

30

31

32

33

34

35

36

37

38

39

40

41

42

43

44

Recent studies have identified circular RNAs (circRNAs) expressed from the Epstein Barr virus (EBV) and Kaposi's sarcoma herpesvirus (KSHV) human DNA tumor viruses. To gain initial insights into the potential relevance of EBV circRNAs in virus biology and disease, we assessed the circRNAome of the interspecies homologue, rhesus macaque lymphocryptovirus (rLCV) in a naturally occurring lymphoma from a simian immunodeficiency (SIV) virus infected rhesus macaque. This analysis revealed rLCV orthologs of the latencyassociated EBV circular RNAs, circRPMS1_E4_E3a and circEBNA_U. Also identified in two samples displaying unusually high lytic gene expression was a novel rLCV circRNA that contains both conserved and rLCV-specific RPMS1 exons and whose backsplice junctions flank an rLCV lytic origin of replication (OriLyt). Analysis of a lytic infection model for the murid herpesvirus 68 (MHV68) rhadinovirus identified a cluster of circRNAs near an MHV68 lytic origin of replication with the most abundant of these, circM11_ORF69 spanning the OriLyt. Lastly, analysis of KSHV latency and reactivation models revealed the latency associated circRNA originating from the vIRF4 gene as the predominant viral circRNA. Together, this study broadens our appreciation for circRNA repertoires in the lymphocryptovirus and rhadinovirus genera of gammaherpesviruses and provides evolutionary support for viral circRNA functions in latency and viral replication.

46

47

48

49

50

51

52

53

54

55

56

IMPORTANCE

Infection with oncogenic gammaherpesviruses leads to long-term viral persistence through a dynamic interplay between the virus and the host immune system. Critical for remodeling of the host cell environment after the immune responses are viral non-coding RNAs that modulate host signaling pathways without attracting adaptive immune recognition. Despite the importance of non-coding RNAs in persistent infection, the circRNA class of non-coding RNAs has only recently been identified in gammaherpesviruses. Accordingly, their roles in virus infection and associated oncogenesis are unknown. Here we report evolutionary conservation of EBV encoded circRNAs by assessing the circRNAome in rLCV infected lymphomas from an SIV infected rhesus macaque and we report latent and lytic circRNAs from KSHV and MHV68. These experiments demonstrate utilization of the circular RNA class of RNAs across 4 members of the gammaherpesvirus subfamily and they identify orthologs and potential homoplastic circRNAs, implying conserved circRNA functions in virus biology and associated malignancies.

Downloaded from http://jvi.asm.org/ on January 4, 2019 by guest

58

59

60

61

62

63

64

65

66

67

68

69

70

71

72

Downloaded from http://jvi.asm.org/ on January 4, 2019 by guest

INTRODUCTION

The oncogenic properties of tumor-associated gammaherpesviruses are manifested through repertoires of viral genes expressed in their respective associated cancers. Nevertheless, expression of oncogenic Epstein Barr virus (EBV) protein coding latency genes is suppressed in most EBV associated tumors and/or is variable across tumor types and patients (1-6). Differences in expression of these viral proteins is probably driven in part by the degree and mechanisms of immune privilege that are unique to tissue of origin, tumor site, and between patients. More consistently expressed are EBV latency associated non-coding RNAs, such as the small non-coding RNAs, EBER1 and EBER2, the BamHI A region microRNAs, and the BamHI A region long non-coding RNAs (referred to as RPMS1 and A73) (7-15). The pervasive expression of these non-coding RNAs across most stages of the natural EBV infection cascade presumably reflects the effectiveness of this strategy to modulate the host cell environment without eliciting a substantial adaptive immune response. The pan tissue expression of these viral non-coding RNAs is recapitulated across EBV-associated cancer types and patients where their expression likely contributes broadly to the tumor phenotype in a relatively immunologically transparent manner. Appreciating the repertoire and functions of viral non-coding RNAs is therefore critical for efforts to understand the mechanisms of viral oncogenesis and for the development of therapeutic strategies to target virus-associated cancers.

73

74

75

76

77

78

79

80

81

82

83

84

Circular RNAs (circRNAs) are a recently appreciated class of primarily non-coding RNAs that have been detected across the 5 kingdoms of life (16-22). circRNAs are formed through backsplicing of 3' splice donor sequences to upstream 5' splice acceptor sequences to generate closed circular RNAs that have increased stability due to a lack of sensitivity to exonucleases. With their unique structure and increased stability, circRNAs likely play distinct functions in the cell and seem uniquely suitable for modulating pathways that require sustained effector signaling. Utilizing a series of B-cell and stomach cancer cell models representing the three major EBV latency gene expression programs (latency type I, type II and type III) and viral reactivation, we have recently reported that EBV encodes a diverse repertoire of viral circRNAs (23). Some EBV circRNAs were uniquely associated with latency type- and/or reactivation whereas others were broadly expressed across tissue and tumor types (23). The EBV encoded circRPMS1_E4_E3a and circRPMS1_E4_E2 RNAs, which are derived from the non-coding RPMS1 gene locus, were found to be expressed in all three

latency types and in B-cell and epithelial tumor models. Further, they were found to be expressed in stomach cancer and post-transplant lymphoproliferative disease (PTLD) patient specimens (23, 24). A lower abundance viral circRNA, circEBNA_U, derived from the Epstein Barr nuclear antigen (EBNA) locus, was detected in Bcells displaying both type I and type III latency and was detected during reactivation (23).

89

90

91

92

93

94

95

96

97

98

99

100

101

102

103

104

105

106

107

85

86

87

88

To gain insight into the potential significance of EBV circular RNAs, we performed a limited evolutionary study utilizing the rhesus macaque lymphocyrptovirus (rLCV) model which shows nearly identical gene organization across the genome but which shares only 65% nucleotide homology with EBV (25). Utilizing three different tumor specimens from a naturally occurring SIV-associated rhesus macaque lymphoma(s), we found high levels of rLCV gene expression indicating a likely rLCV etiology. Assessment of the rLCV circRNAome showed low but detectable expression of the rLCV counterpart to the EBV circEBNA_U circRNA in all three samples. More robust detection of an EBV circRPMS1_E4_E3a homologue displaying both common and rLCV-specific RPMS1 exon utilization was also observed. An additional rLCV RPMS1 circular RNA, circRPMS1 E2b E1b, surrounds a lytic origin of replication and appears to be uniquely detected in rLCV but not EBV. We also performed circRNA analyses of two more distantly related gammaherpesviruses, the Kaposi's sarcoma herpesvirus (KSHV) and murid herpesvirus 68 (MHV68) rhadinoviruses. This analysis identified a latently expressed circular RNA derived from the vIRF4 gene, consistent with previous studies (24, 26), and a lytic MHV68 circular RNA that encompasses one of MHV68's lytic origins of replication. Together, this work demonstrates the conservation of circRNA utilization as a potential mechanism to facilitate cell signaling in the absence of affecting an adaptive immune response. Further, we identify viral circRNAs and features that are conserved between the EBV and rLCV lymphocryptoviruses, with the finding of an EBV circRPMS1_E4_E3a homologue being particularly noteworthy due to the broad detection of circRPMS1_E4_E3a across latency and cell types and in the natural in vivo tumor setting (23, 24, 26).

RESULTS

108

109

110

111

112

113

114

115

116

117

118

119

120

121

122

123

124

125

127

128

129

130

131

132

133

134

135

Rhesus SIV/LCV lymphoma model. To investigate conservation of recently identified EBV circRNAs (23, 24), we utilized the rhesus lymphocryptovirus (rLCV) model which despite remarkably similar genomic organization, shares only 65% nucleotide homology with EBV (25). This analysis was performed using tumor tissues from naturally occurring lymphomas in a simian immunodeficiency virus (SIV) infected Indian rhesus macague. This adult male macaque (14 years), negative for the MHC-I alleles Mamu-A*01, Mamu B*08 and Mamu B*17 received twice-daily oral doses (60 mg, 30 mg) of dimethylfumarate for 7 days prior to intravenous inoculation with SIVmac251 (100 TCID50). The animal then received three successive doses of the anti-CD8 antibody MT807R (10 mg/kg, 5 mg/kg, 5 mg/kg) at days 6, 9, and 13 post-infection. Plasma and cerebrospinal fluid (CSF) samples were collected at several time points up until the day of autopsy (day 84 post-infection) for analysis of SIV RNA levels (Fig. 1A). As expected, CSF SIV RNA levels were ~ 1 log lower than those of plasma and at necropsy (d84) plasma SIV load was 1.9 x 10⁹. Two effaced lymph node sections and a white nodule located next to a cut margin of the jejunum (Fig. 1B) were excised and flash frozen. RNA was isolated from snap frozen tissues and the RNAs were subjected to both polyA- and RNase R-sequencing. Mapping of the polyA-seg reads from each sample to the cellular plus rLCV genomes (25) demonstrated robust viral transcript detection with 224, 3744, and 4942 viral reads per million mapped reads (Fig. 1C). These values are comparable to or higher than EBV RNA detection rates in clinical isolates of EBV positive lymphomas and stomach cancers (2, 3, 6) indicating likely true tumor cell infection and virus etiology.

126

While the bulk of the reading frames across the rLCV genome have been annotated (25), rLCV transcript structures, to our knowledge, have not been globally assessed (as has been done for EBV (27)). Further, the non-coding RPMS1 and A73 genes found in EBV have not been identified or annotated in the rLCV genome build (25). Since we had previously identified EBV circRNAs derived from the EBV RPMS1 locus both in cell lines and in stomach cancer tumor tissue (23), we first utilized our polyA-seg and RNase R-seg coverage and splice junction data to produce a tentative working exonic structure for both of these transcripts (Fig. 2, see https://github.com/flemingtonlab/public/blob/master/annotation/rLCV_inverted.fa_and https://github.com/flemingtonlab/public/blob/master/annotation/rLCV inverted.bed for resulting rLCV genome fasta and annotation files).

Using the polyA-sequencing data, we first assessed the viral transcription profiles for each sample. Notable in the two lymph node samples was high expression of lytic genes with particularly high expression of many early genes such as BMLF1, BMRF2, and BNLF2a (Fig. 1D). The jejunum tumor sample displayed lower but readily detectable early lytic gene expression but was distinct in its utilization of the Cp latency promoter, expression of EBNA2, low level expression of the other type III latency EBNAs, -1, -3A, -3B, and -3C and low levels of LMP2 (Fig. 1D). This indicated that among these three specimens, at least two distinct viral transcription programs were at our disposal for interrogating viral circRNA expression.

144 145

146

147

148

149

150

151

152

153

136

137

138

139

140

141

142

143

Detection of viral circRNAs in rLCV lymphomas. To assess the rLCV circRNAome in these LCV+ lymphoma samples, we analyzed the three RNase R-sequencing data sets for backsplicing across the rLCV genome using find circ (28). Backsplice reads extending from RPMS1 exons 5 to exon 3a were found to be the most abundant and were observed in all three samples (Fig. 3). Notably, two exon 5 to exon 3a backsplice isoforms were detected that were derived from distinct exon 5 splice donor sites located only 7 bases apart (Fig. 3; denoted as E5' and E5). Backspliced reads extending from RPMS1 exons 2b to 1b were also observed in the two "lytic" tumor samples and again, two backsplice variants were detected, derived from alternative splice donor sites in exon 2b (Fig. 3). Lastly, we detected backsplice reads mapping to the EBNA U exon (29, 30), revealing an rLCV homologue of the previously reported EBV circEBNA_U circular RNA (Fig. 3) (23).

154 155

156

157

158

159

160

161

To validate these findings in silico, we performed alignments to a genome containing the Macaca mulatta cellular chromosomes plus conjoined backsplice exon junction sequences for each of these putative circRNAs. Junction spanning reads with at least a 12 base overlap and a minimum of 90% homology on each side of the junction were then extracted and loaded onto the integrative genomics viewer (IGV) (31) for visualization. A staggered distribution of junction spanning reads were detected for each backsplice call shown in Fig. 3 (data not shown) demonstrating that they represent bona fide splicing events and not random cDNA ligation chimeras generated during library preparation.

162

rLCV circRPMS1 E5 E3a, an rLCV ortholog of EBV circRPMS1 E4 E3a. To validate the closed circular nature of circRPMS1_E5_E3a (Fig. 4A), RNAs from all three lymphoma samples were subjected to RNase R treatment and exons 5 and 3a specific divergent primers were used to PCR across the backsplice junction (Fig. 4B). While linear ACTB RNAs were found to be susceptible to RNase R digestion, no decrease in the RPMS1 exons 5-to-3a PCR signal was observed with RNase R treated RNAs (Fig. 4B). Cloning and sequencing the RPMS1 E5-to-E3a PCR fragments revealed representation of both the RPMS1 E5'-to-E3a and the RPMS1 E5-to-E3a backsplice junctions.

170 171

172

173

174

175

176

177

178

179

163

164

165

166

167

168

169

Visual assessment of RNase R-seq coverage across the RPMS1 exon 3a to exon 5 genomic region showed enriched coverage over exons 3a, 4 and 5 (data not shown). Further, forward spliced junction reads spanning exons 3a to 4 and exons 4 to 5 were also readily detected in the RNase R-seq data (data not shown). This suggested that circRPMS1_E5' E3a and circRPMS1_E5 E3a are composed of forward spliced exons 3a, 4 and 5 (Fig. 4). To further assess this potential exon configuration, leftward primers specific to exons 3a, 4 and 5 and a common exon 5 rightward primer were used to RT-PCR from each of the three tumor samples (Fig. 4B). PCR fragment sizes were consistent with the circRPMS1_E5'_E3a and/or circRPMS1_E5_E3a containing consecutively forward spliced exons 3a-to-4-to-5 (Fig. 4B, bottom panel) and this was confirmed by sequencing each of the amplified fragments.

180

181

182

183

184

185

186

187

188

Together, these results indicate that circRPMS1 E5' E3a and circRPMS1 E5 E3a are derived from alternative splice donors in RPMS1 exon 5, they are expressed in all three tumor samples, and they contain consecutively forward spliced exons 3a, 4, and 5. While the separate evolutionary tracks of EBV and rLCV have led to species-specific circularization of some of the RPMS1 exons (for example, EBV-specific utilization of exon E3b and rLCV-specific utilization of exon 5) and distinct splice donor utilization for exon 4 (Figs. 2 and 4), the common seguences of exons 3a and 4 show high homology (88% and 92%) (Fig. 2). We therefore hypothesize that the rLCV circRPMS1_E5_E3a is a functional homologue of EBV circRPMS1_E4_E3a with potentially related roles in their respective virus infection cycles.

189

191

192

193

194

195

196

197

198

199

200

rLCV circRPMS1 E2b E1b spanning a lytic origin of replication. Investigation of RPMS1 coverage and splicing information from polyA- and RNase R-sequencing data sets revealed divergent exon usage downstream from exon 1b (Figs. 2 and 5A). In rLCV, there is no evidence for the usage of the EBV RPMS1 exon 2. On the other hand, two rLCV-specific upstream "exon 2s" are detected in the two lytic SIV/rLCV lymphoma samples (Figs. 2 and 5A), with exon 2a being located within a lytic origin of replication. Whereas we found no evidence of EBV backsplicing to RPMS1 exon 1b (23), in the two lytic rLCV samples, we detected backsplicing from exons 2b to 1b (Figs. 3, 4, and 5). Using divergent primers designed against exons 2b and 1b, a product of the appropriate size was amplified, with higher levels of detection observed in the two lytic tumors (T1 and T3) (Fig. 5B). Cloning and sequencing of these fragments verified both exon 2b splice donor to exon 1b backsplice junctions shown in Fig. 3. The respective RNAs were resistant to RNase R digestion (Fig. 5B) indicating the circular nature of RNAs derived from RPMS1 exon 2b to exon 1b backsplicing.

201 202

203

204

205

206

207

208

209

210

211

212

213

214

215

216

To assess the exonic structure of circular RNAs containing the exon 2b to exon 1b backsplices, we designed exon 1b, 2a, and 2b leftward PCR primers and a common exon 2b rightward PCR primer (Fig. 5). RT-PCR with these three primer pairings resulted in fragment sizes that were consistent with an exon 1b, 2a, and 2b containing circular RNA, and sequencing of these fragments validated this assessment. This analysis indicated that circRPMS1_E2b/E2b'_E1b RNAs contain canonical forward spliced exons 1b-to-2a-to-2b. With the exon 2b leftward primer, however, we also detected a lower molecular weight PCR fragment (Fig. 5C) that, upon sequencing, was found to result from exon 2a exon skipping. Therefore, at least two circRPMS1_E2b/E2b'_E1b isoforms were detected differing in the inclusion or skipping of exon 2a. Lastly, while visualization of RNase R-seq coverage across this region showed elevated coverage at these exonic regions, there is relatively high intronic coverage. We therefore do not preclude the possibility of intron retention for some circRPMS1_E2b/E2b'_E1b isoforms (these products would be larger than the spliced products and PCR amplification is expected to be less efficient than their spliced counterparts). Together, this analysis demonstrates the expression of a novel set of RPMS1 circular RNA isoforms spanning the lytic origin of replication that were not observed previously in our EBV circular RNAome analysis (23).

rLCV circEBNA U. Based on analysis of the polyA- and RNase R-seq splicing and coverage data, rLCV EBNA transcripts splice to a small non-coding exon with a high degree of exonic, flanking intronic, and splice junction sequence homology to the EBV non-coding EBNA U exon (data not shown). In our previous analysis of EBV circRNAs, we detected backsplicing of the EBNA U exon in most lymphoma-derived cell lines (23). Backsplicing analysis of the rLCV RNase R-seg data similarly showed evidence of backsplicing of the rLCV EBNA U exon (Fig. 3). Using divergent primers to PCR across the backsplice region, the appropriate sized band was amplified in all three samples and was found by Sanger sequencing to validate the backspliced junction (Fig. 6). Further, RNAs containing the EBNA U backsplice were resistant to RNase R digestion confirming the closed circular nature of the rLCV circEBNA_U (Fig. 6). Therefore, like it's EBV counterpart, rLCV expresses a latency associated circEBNA_U circular RNA in lymphomas.

227 228

229

230

231

232

233

217

218

219

220

221

222

223

224

225

226

Detection of latently expressed circular vIRF4 transcript in KSHV latently infected cells of lymphoid, endothelial and epithelial origin. To assess whether circular RNAs are expressed from a divergent human gamma herpesvirus, we performed RNase R-seq on either untreated or TPA treated KSHV positive BCBL-1 cells. Besides a cluster of low abundance (5 reads or less) backsplice calls mapping to the PAN transcript (24, 26) and a few other sporadically distributed loci in TPA treated BCBL1 cells, a predominant latency associated backsplice was detected at the vIRF4 locus (32, 33) with the backsplice junctions flanking a known forward splice junction (Fig. 7) which was also detected recently (24, 26). This backsplice was confirmed in silico through realignment of reads to conjoined backsplice junction sequences (data not shown). Coverage was restricted to the confines of the backsplice junctions with a decrease in coverage observed within the intron (Fig. 7). Notably, although vIRF4 is defined as a lytic gene (34, 35), there is no increase in backsplice junctions observed in reactivation conditions (TPA treatment). This suggests that there is a unique transcriptional mechanism that gives rise to the observed latency expression of circvIRF4, perhaps from a previously unrecognized latency promoter.

241

242

243

244

The circular nature of the RNA containing the vIRF4 backsplice junction was verified by showing resistance to RNase R digestions (Fig. 7B). Further, excising the bands from RT-PCR reactions using three different primer pairs (PP 1, PP 2, and PP 3, see Fig. 7B) validated the backsplice junction. Notably, the leftward primer for the primer pair, PP3 is located to the right of the forward splice junction and using this PP3 primer pair, two bands were observed in BCBL1, and KSHV infected TIVE and iSLK cells. Sequencing of both of these bands revealed that the lower band represents a circvIRF4 isoform with the intron spliced out while the upper band represents a circvIRF4 isoform that retains this intron. Therefore, two isoforms of circvIRF4 are generated during latency in each of these cell line models.

250 251

252

253

254

255

256

257

258

259

260

261

262

263

264

265

266

267

268

245

246

247

248

249

Circlular RNA expression at the MHV68 OriLyt locus. We next assessed circRNA expression in an evolutionarily distinct rhadinovirus family member, MHV68. For this, we analyzed latently infected HE2.1 Bcells (36) and we analyzed lytic replication through infection of NIH 3T12 cells with MHV68 (18 hours after infection at an MOI of 5). We detected no viral backsplice junctions in latent HE2.1 cells, possibly due to the lack of expression of most latency genes outside of the tmers during latency in these cells. In lytically infected NIH 3T12 cells, we detected very low backsplice read numbers scattered across the genome and we detected a particularly high density cluster of more than 40 lowly detected backsplices near an MHV68 OriLyt (37-39) and a higher abundance intergenic ca. 11 kb backsplice extending from the M11 gene to the ORF69 gene whose backsplice junctions spanned the OriLyt (Fig. 8A). The circM11_ORF69 backsplice was validated in silico through realignment to the conjoined backsplice junction (data not shown). Further, circM11_ORF69 was found to be resistant to RNase R digestion (Fig. 8B and C). Analysis of RNase R sequencing data showed good coverage across the 11 kb region spanning the backsplice junctions except for the repeat region (repeat regions commonly cause a lack of RNA-seq coverage likely due to technical reasons). Additional nested primers within ORF69 resulted in PCR products of the appropriate sizes (Fig. 8C), indicating inclusion of these ORF69 sequences in circM11_ORF69. Forward spliced reads were detected in the RNase R-seq data that extended into M11 suggesting that there are a number of spliced isoforms (Fig. 8A). Nevertheless, barring other undetected splice sites, this data suggests that forward spliced and non-spliced isoforms of circM11_ORF69 could range in size from more than 8 kb to greater than 11 kb long.

DISCUSSION

270

271

272

273

274

275

276

277

278

269

Given the recently discovered ubiquitous nature of circRNAs across all kingdoms of life, it is not unexpected to find that gammaherpesviruses of both the lymphocryptovirus and rhadinovirus genera encode genes that give rise to circRNAs. Despite this, however, it is important to document this previously unappreciated class of gammaherpesviral transcripts so they can be included in our efforts to understand the mechanisms of both the natural infection cycles of these viruses and their contributions to cancer. Further, the identification of individual circRNAs and our initial characterizations of their exonic structures and evolutionary conservation should provide foundational information from which to begin investigations into the functions of these RNAs in natural virus biology and disease.

279 280

281

282

283

284

285

286

287

288

289

From an evolutionary standpoint, our studies identify two conserved lymphocryptovirus circRNAs, circEBNA_U and circRPMS1 E4 E3a (EBV)/circRPMS1 E5/E5' E3a (rLCV). Despite being lowly detected, we found EBV circEBNA_U expression in type I and type III latency B-cell models (although we have yet to detect it in any stomach cancer model tested to date) (23) and we detected the rLCV encoded circEBNA_U in all three lymphoma samples investigated here. Its low expression could support the idea that circEBNA U forms due to processing inefficiencies associated of upstream and/or downstream linear splicing. Even in this case, though, the evolutionary conservation between two lineages supports a possible functional significance. It is also notable that the coverage of the EBNA U exon and all other exons that make up the EBNA1 transcript is low in our PolyA-seq data from most latency type I and type II models we have tested. The low abundance of circEBNA_U is therefore consistent with the overall expression of its parental transcript.

290

291

292

293

294

295

296

Visualization of the EBNA U and flanking sequence homology between EBV and rLCV shows a fairly divergent center of exon U with greater homology near the end sequences, extending into the intronic regions (data not shown). The high homology at the intronic and exonic regions within and proximal to the splice junctions presumably maintains the structure and sequence motifs necessary to retain conserved splicing factor and splicing enhancer factor interactions which may in turn account for conservation of circularization. It is also notable that circular RNAs become loaded with the splicing factors involved in their genesis (40-42). As such,

the observed sequence conservation of flanking introns and splice junction regions is consistent with the loading of many of the same factors onto circEBNA_U for both EBV and rLCV. Since these associated splicing factor and splicing enhancer factor cargo/effectors likely play a key roles in facilitating circRNA function, this suggests conserved biological roles for circEBNA U across these two viral relatives.

301 302

303

304

305

306

307

308

309

310

311

312

313

297

298

299

300

One of the notable observations arising from our analysis of the rLCV RPMS1 exon configurations was the finding of substantial variations in exon utilization between rLCV and EBV (Fig. 2). EBV utilizes two exons, E2 and E3b that we find no evidence for in any of the three rLCV lymphoma samples. Conversely, splicing analysis in the rLCV lymphoma samples supported the existence of four novel exons not detected in EBV (Fig. 2). Among RPMS1 exons that are not part of the A73 isoform (i.e. are unique to the RPMS1 isoform), it is notable that in addition to differential utilization of exons, there is relatively low homology of exons 1, 1a and 1b. In contrast, the exons, 3a and 4, which are components of the EBV circRPMS1_E4_E3a and rLCV circRPMS1 E5 E3a circular RNAs display 88% and 92% homology (Fig. 2) with homologies extending into the intronic and splice junction signaling sequences. While the high homologies between these RPMS1 exonic regions may be driven largely by selective pressure to maintain the LF2 open reading frame on the opposite strand, the homolgous exonic and flanking intronic sequences important for loading of splicing factors to the respective circRNAs would nevertheless likely facilitate similar functioning of the EBV circRPMS1_E4_E3a and rLCV circRPMS1_E5_E3a circular RNAs through their bound protein cargo.

315 316

317

318

319

320

321

322

323

We previously demonstrated the expression of EBV circRPMS1 E4 E3a and circRPMS1 E4 E2 in two stomach cancer patient samples (23). Assessment of 4 additional stomach cancer patient samples similarly show expression of both circRPMS1_E4_E3a and circRPMS1_E4_E2 (Fig 9, T3 and T5 are samples that we previously assayed (23) while T1, T2, T4, and T6 represent findings in 4 new stomach cancer specimens). In addition, Toptan et al (24) demonstrated expression of circRPMS1_E4_E3a and circRPMS1_E4_E2 in a panel of post-transplant lymphoproliferative disease patient specimens. The findings of broad expression of circRPMS1_E4_E3a and circRPMS1_E4_E2 across a panel of type II, type II, and type III cell lines (23), in primary stomach cancer and PTLD patient samples (Fig 9, and (23, 24)), and our findings here identifying an

346

347

348

349

350

351

rLCV homologue in clinical lymphoma specimens speaks to a likely conserved, ubiquitious and clinically relevant potential function for these viral circRNAs in EBV/rLCV biology and associated cancers.

325 326

327

328

329

330

331

332

333

334

335

336

337

338

339

340

324

We previously identified a highly expressed EBV circRNA derived from the lytic BHLF1 gene located next to one of the two EBV lytic origins of replication (23). In reactivation conditions, this circRNA was among the top 5 most abundant circRNAs in the cell (43) and in the majority of latency conditions, low level circBHLF1 was detected, possibly due to a small percentage of spontaneously reactivating cells among the latency population or low level latency expression (44). Based on findings of Rennekamp et al (45) that some undefined BHLF1 RNA isoforms bind to and activate the lytic origin of replication, we previously hypothesized that the circular BHLF1 isoforms are reasonable candidates for such a role (23). In our analysis of the rLCV circRNAome, however, we did not detect backsplice reads mapping to the corresponding BHLF1 region of rLCV in any of the three lymphoma samples assayed here despite the observation that two of these samples displayed relatively robust levels of lytic gene expression. Nevertheless, it is notable that circRPMS1 E2b E1b spans the other rLCV lytic origin of replication and is detected uniquely in the two samples displaying lytic activity but not in the sample with the more latent viral transcription program. In addition, we found that the predominant backsplices detected in MHV68 was a cluster arising from near one of the MHV68 lytic origins of replication during lytic infection, with the junctions of the most abundant circular RNA, circM11_ORF69, spanning this lytic origin of replication (Fig. 8). While these relationships may be coincidental or, the process of replication may drive backsplicing, it also leaves open the possibility of homoplastic evolution of these circRNA/OriLyt pairings with proximal viral circRNAs playing active roles in facilitating lytic viral DNA replication.

Downloaded from http://jvi.asm.org/ on January 4, 2019 by guest

344

The KSHV encoded vIRF4 gene is classified as a lytic gene that plays a role in regulating viral lytic gene expression (32-35, 46, 47). It is notable, however that in latency conditions, our BCBL-1 RNase R-sequencing coverage data shows a strong bias for reads specifically within the confines of the circvIRF4 backsplice junctions (Fig. 7). In reactivation conditions, however, there is an increase in coverage presumably from inefficiently RNase R digested linear vIRF4 transcripts but little increase in the region within the circvIRF4 backsplices. Further, there is no observed increase in the number of backspliced reads in TPA treated cells. This suggests that while vIRF4 linear transcripts are likely induced during reactivation, circvIRF4 is expressed

353

354

355

356

357

358

359

360

361

362

363

364

365

366

as a non-coding latency transcript and may play a role in modulating the host cell environment during latency and in KSHV associated malignancies.

Together, we have shown that both the rhadinovirus and lymphocryptovirus genera of gammaherpesviruses express a diverse set of circRNAs. From this limited evolutionary assessment of the lymphocryptovirus genus, we have been able to identify conservation of circEBNA_U and a variation of the EBV circRPMS1_E4_E3a circular RNA that we have detected nearly universally in our tissue culture models and in primary stomach cancers. Testing of additional rLCV samples (tissue culture and primary tissue models) as well as LCVs with other species tropisms will further address our contention of circEBNA_U and circRPMS1_E4_E3a (EBV)/circRPMS1_E5_E3a(rLCV) conservation and at the same time, may reveal conservation of additional viral circRNAs detected previously for EBV (23). Further, the analysis of other rhadinoviruses that are more closely related to KSHV or MHV68 may yield insights into the possible importance of the KSHV encoded circvIRF4 latency circRNA and the lytic associated MHV68 circM11 ORF69 circRNA. Together, these evolutionary studies will set the stage for beginning investigations into the function and importance of these viral circRNAs in virus biology and associated cancers.

Downloaded from http://jvi.asm.org/ on January 4, 2019 by guest

368

369

370

371

372

373

374

375

376

377

378

379

380

381

MATERIALS AND METHODS

Cell culture and infections. BCBL1 and SNU719 (Korean Cell Line Bank) cells were grown in RPMI 1640 media (Fisher Scientific, catalog no. SH30027) supplemented with 10% fetal bovine serum (FBS) (Thermo Fisher, catalog no. 10437). YCCEL1 cells (Korean Cell Line Bank) were cultured in Eagle's minimum essential medium (EMEM) (ATCC, catalog no. 30-2003) supplemented with 10% fetal bovine serum (FBS) (Thermo Fisher, catalog no. 10437). All cells were cultured at 37°C in a 5% CO₂ incubator. For lytic MHV68 infections, NIH 3T12 cells (grown in Dulbeco's Modified Eagles medium supplemented with 10% fetal bovine serum) were infected with MHV68 at a multiplicity of infection (MOI) of 5 and harvested 18 hrs post-infection for RNA preparation.

Animal model. An adult male (14 years) Indian rhesus macaque (MHC genotype: Mamu-A*02, Mamu-A*08, Mamu-B*01 positive, and Mamu-A*01, Mamu-A*11, Mamu B*03, Mamu B*04, Mamu B*08 and Mamu B*17 negative) received twice-daily oral doses (60 mg, 30 mg) of dimethylfumarate for 7 days prior to intravenous inoculation with SIV (SIVmac251; 100 TCID50). The animal then received three successive doses of anti-CD8 antibody (10 mg/kg, 5 mg/kg, 5 mg/kg) at days 6, 9, and 13 post-infection. Plasma and cerebrospinal fluid (CSF) samples were collected at several time points up until the day of autopsy (day 84 post-infection) for analysis of SIV RNA levels.

382 383

384

385

386

387

388

At autopsy, lymphosarcoma was identified in all lymphoid tissues examined, including the tonsils, and nodes within the jejunum, cecum, and colon. Lymphocytic infiltration was observed in the kidney, liver, adrenal gland, lung, and sciatic nerve, consistent with lymphocytic inflammation. The brain demonstrated granulomatous encephalitis, and multinucleated giant cells were observed in the brain, brainstem, and cervical spinal cord. Mild to moderate amyloidosis was found in the liver and spleen.

389

390

391

392

393

RNA preparations. Whole cell RNA preparations were carried out using TRIzol reagent (Thermo Fisher, catalog no. 15596) according to the vendor's recommended protocol. For tumor and normal tissue, pieces were first ground finely using a mortar and pestle in liquid nitrogen prior to disruption with TRIzol reagent. Nuclear and cytoplasmic RNAs were isolated using the Cytoplasmic & Nuclear RNA Purification Kit from

395

396

397

398

399

400

401

402

403

404

405

406

407

408

409

410

411

412

413

414

415

416

417

418

419

420

Norgen Biotek Corp. (catalog no. 21000) according to the vendor's protocol. All RNA preparations were subjected to DNase treatment twice using the DNA-free kit (Thermo Fisher, catalog no. AM1906).

RNA-sequencing. RNA-sequencing was performed at the Beijing Genomics Institute (BGI). For polyA-seq. RNAs were selected using a poly dT column, and for RNase R-seq, RNAs were subjected to DNA and rRNA depletion, followed by linear RNA depletion using RNase R. For all sequencing experiments, Truseg stranded libraries were generated and sequenced using 2x100 base sequencing on a HiSeg 4000 system. All RNAsequencing data has been deposited to the NCBI GEO public database (Accession number GSE116675).

Backsplice junction analysis. Backsplicing was analyzed using find_circ (28) with default parameters. For analysis of BCBL1 cell RNase R-seq data, alignments were carried out using the human hg38 genome build plus the NC_009333 human herpesvirus 8 genome (48). Alignments for backsplicing analysis of rhesus lymphoma samples was performed using the macaca mulatta mmul8.01 genome build plus the NC 006146 macacine gammaherpesvirus 4 genome (25) which was split at nucleotide position 102091 rather than the beginning of the terminal repeats (position 1) to allow for assessment of splicing across the LMP2 locus that spans the terminal repeats. For MHV68 backsplicing analyses, RNase R-seq data was aligned to the mouse mm10 genome build plus the MHV68 genome (49). For in silico validations, STAR (50) genome indices were generated containing the human hg38 (BCBL1), macaca mulatta (Rhesus lymphomas), or the murine mm10 genome builds plus the respective conjoined backsplice junctions for KSHV, LCV, or MHV68 identified by find circ. Raw fastg files were aligned to the respective genome indices using STAR (--outFilterMultimapNmax 20 --outSAMtype BAM SortedByCoordinate --outWigType wiggle --outWigNorm None), reads spanning backsplice junctions with a minimum of 12 base overlap (minimum of 90% homology) on each side of the junction were pulled out for visualization on the Integrative Genomics Viewer (IGV) (31) and the number of reads mapping to each junction were quantified for reporting.

Splice junction and expression exon structure plots. For canonical splicing and coverage display, RNAseq data from polyA+ or RNase R sequencing libraries were analyzed by STAR alignment against the respective cellular plus viral genomes using STAR --outFilterMultimapNmax 20 --outSAMtype BAM SortedByCoordinate --outWigType wiggle --outWigNorm None). Splice junction data from .SJ files and wiggle output files were used to generate junction read numbers and coverage information. Backsplice read counts

447

Rhesus RPMS1 E4 rev:

Rhesus RPMS1 E5 rev:

421	were extracted from .bed junction count file	s derived from find_circ output. Forward splicing, coverage and			
422	backsplicing, were visualized together usin	g the software, circleVis (Ungerleider and Flemington, submitted).			
423	For these plots (Figs. 4A, 7A and 8A), exor	n level coverage is represented by color intensity with canonical and			
424	backsplice junction curves plotted above ar	nd below the exon diagram, respectively.			
425	RNase R resistance analysis. 5 ug of tota	al RNA was incubated with or without 60 units of RNase R (Lucigen,			
426	catalog no. RNR07250). Briefly, no (control) or 1.5 ul RNase R (30 units) and 3 ul of 10X RNase R buffer were			
427	added to 5 ug of RNA in a total volume of 30ul and incubated in a 37°C water bath for 30 minutes. Either no				
428	(control) or 1.5 ul (30 units) more RNase R was added to the reactions and incubated for an additional 1.5				
429	hours in a 37°C water bath. RNAs were then cleaned and concentrated using the RNA Clean & Concentrator-5				
430	kit (Zymo Research, catalog no. R1015) and eluted in 10ul H ₂ O, 9ul of which was used for cDNA preparations				
431	(below).				
432					
433	RT-PCR. cDNA was synthesized using SuperScript IV First-strand Synthesis System (Thermo Fisher, catalog				
434	no. 18091) or ProtoScript II Reverse Transcriptase (New England Biolabs, MA, USA) and the cDNAs were				
435	amplified by taq-PCR (Thermo Fisher, catalog no. 11304) following the vendor's protocol. PCR products were				
436	run on a 1% agarose gel at room temperature. PCR products were cut out and purified using the NucleoSpin				
437	Gel & PCR Clean-up Kit (Clontech, catalog no. 740609). The resulting PCR fragments were cloned into the				
438	pCR4-TOPO vector (Thermo Fisher, catalog no. 450030) and the inserts were Sanger sequenced.				
439					
440	PCR primers:				
441	GAPDH for (human/mouse):	5'-ACCACAGTCCATGCCATCAC			
442	GAPDH for (Rhesus):	5'-TGGCCAAGGTCATCCATGACA			
443	GAPDH rev (human/mouse/Rhesus):	5'-TCCACCACCCTGTTGCTGTA			
444	Rhesus RPMS1 E5 for:	5'-GAGCACCAGGGCAAAGAC			
445	Rhesus RPMS1 E3a rev:	5'-CACGACTCCGTTCCTGAAGT			

5'-AGGAGCCCATGCAGCACTA

5'-GCTATCTCCTGGCGGGTATC

448	Rhesus RPMS1 E1b for:	5'- AAGCACCACAGACACGAGA
449	Rhesus RPMS1 E2a for:	5'-GGAAGCGTGGACCCAGA
450	Rhesus RPMS1 E2b for:	5'-GCCAGGACTGGTACCTGAGA
451	Rhesus RPMS1 E1b rev:	5'-GGTTGGGCCGTTTCCTAC
452	Rhesus EBNA-U for:	5'-AGACCGTCGCGTCGTAGA
453	Rhesus EBNA-U rev:	5'-GCAGAATCAGCTCTCCCAGA
454	KSHV circvIRF4-PP1-for:	5'-CTCCGTGTGGATACCAGTGA
455	KSHV circvIRF4-PP1-rev:	5'-TGGTTCCACGCAACAGTCT
456	KSHV circvIRF4-PP2-for:	5'-AGAACAAAGCTACGAGGAGGCA
457	KSHV circvIRF4-PP2-rev:	5'-GAATACCAGCCAGGCGGGATA
458	KSHV circvIRF4-PP3-for:	5'-AACCACGGCTACGCGACG
459	KSHV circvIRF4-PP3-rev:	5'-TGCATTGGGGGGGACAAC
460	MHV68 circM11_ORF69-PP1-for:	5'-GGCACTATGACAGCGTTTACC
461	MHV68 circM11_ORF69-PP1-rev:	5'-CTCTCGCCAGAGCAGGAT
462	MHV68 circM11_ORF69-PP2-for:	5'-ATGAGTCATAAGAAAAGCGGGA-3'
463	MHV68 circM11_ORF69-PP3-for:	5'-TCGCTGCGATAGATCATCTG-3',
464	MHV68 circM11_ORF69-PP4-for:	5'-TGCTCCTCCACAAAGGTATG-3'
465	MHV68 circM11_ORF69-PP2,3,4-rev:	5'-ATGGAGCAGAGCCTCCTCACACA-3'
466	EBV circRPMS1 E4 forward:	5'-CTAGTGCTGCATGGGCTCCT
467	EBV circRPMS1 E3a reverse:	5'-GTCATACGCCCGTATTCACA
468		

ACKNOWLEDGMENTS

This work was supported by the National Institutes of health grants, R01Al101046 (EKF), R01Al106676 (EKF),
R01CA188609 (YD), R00GM112877 (WNM), P20GM121288 (ZL), R01AI108407 (ST), R01CA119917 (RR),
and P01CA214091 (RR, ST, and EKF) and the Department of Defense grants, W81XWH-16-1-0318 (EKF),
W81XWH-16-1-0317 (YD). The funders had no role in study design, data collection and analysis, decision to
publish, or preparation of the manuscript. The authors, Teresa A. Lehman and Michael B. Seddon are currently
under the employment of ReproCELL Incorporated. ReproCELL Incorporated provided funds, resources and
equipment to conduct some of the studies and provided salary and benefits for Teresa A. Lehman and Michael
B. Seddon. This does not alter our adherence to all Journal of Virology policies on sharing data and materials.

FIGURE LEGENDS

FIG 1. A) SIV titers in cerebral spinal fluid (CSF) and plasma through 84 days post-SIV infection. B) Hematoxylin and eosin (H&E) staining of lymphoma slides show high tumor cell distributions. C) rLCV reads per million mapped reads from polyA RNA-seq for each lymphoma specimen (T1 - tumor 1, T2 - tumor 2, T3 tumor 3). D) rLCV gene expression in lymphoma samples using the lytic gene classification scheme reported by Djavadian et al. (51). Expression plotted as log2 (transcripts per million (TPM) total cellular plus viral transcripts +1).

485 486

487

488

478

479

480

481

482

483

484

FIG 2. Schematic comparison of exon architecture of RPMS1/A73 locus for EBV and rLCV. Orthologous exons are connected by grey shadings. EBV and rLCV microRNAs (10, 52) are represented by aquamarine vertical bars.

489 490

491

492

493

494

495

496

FIG 3. rLCV circular RNAs identified in lymphoma specimens. Genome coordinates are with respect to the NC_006146 macacine gammaherpesvirus 4 genome genome (25) in which the genome start position was shifted to nulceotide position 102091 of NC_006146 (as described in the materials and methods section) to allow for better assessment of LMP2A transcripts that spans the genome split point of NC 006146. Color intensity represents number of read counts for each backsplice junction for each lymphoma sample (T1, T2, and T3). Positions of the E5, E5', E2b and E2b' splice donor junctions are marked on the respective sequences.

497

498

499

500

501

502

503

504

505

FIG 4. Validation and structure of rLCV circRPMS1_E5_E3a. A) Graphical presentation of splicing and exon specific coverage at the rLCV RPMS1/A73 locus for lymphoma sample T1. To provide a linear RPMS1 expression context, backsplicing read counts (under arches) derived from RNase R-seq datasets are plotted with forward splicing (over arches) and coverage data (exon color intensity) derived from polyA-seg datasets. The number of arches (forward- and back-splicing) correspond to the number of junction spanning reads. Exon shading intensity reflects relative coverage levels across exons and. Aquamarine vertical bars represent rLCV microRNAs (10, 52). B) Validation of circular nature and structure of rLCV circRPMS1_E5_E3a. The schematic illustrates the structural conservation between rLCV circRPMS1_E5_E3a and EBV circRPMS1_E4_E3a.

Upper gels show RNase R resistance of circRPMS1_E5_E3a (E3a leftward primer and E5 rightward primer) but not linear GAPDH. Lower panel shows PCR analysis using divergent primers, exon 3a, 4, or 5 reverse primers and a common exon 5 forward primer (see schematic), demonstrating the exon 3a-to-4-to-5-to-3a configuration. PCR fragments were cloned and sequenced to validate appropriate forward and backsplice junctions.

511 512

513

514

515

516

517

518

519

520

506

507

508

509

510

FIG 5. Analysis of rLCV circRPMS1_E2b_E1b. A) Schematic illustrates exonic structure of circRPMS1_E2b_E1b isoforms and the structural relationship with the EBV RPMS1 locus. B) RNase R resistance of circRPMS1_E2b_E1b. PCR was performed using exon 2b and 1b divergent primers to PCR across the backsplice junction. cDNAs used in Fig. 3B were used here and the GAPDH PCR shown in Fig. 3b serves as a control for the successful RNase R digestion of linear RNAs. C) Divergent PCR using exon 2b, 1b, or 2a reverse primers and a common exon 2b forward primer, demonstrating the exon 2b-to-1b-to-2a-to-2b exon configuration. Also revealed in this analysis was an exon 2a skipped isoform that was observed using the E2b leftward and rightward primers (delta E2a). PCR fragments were cloned and sequenced to validate appropriate forward and backsplice junctions.

Downloaded from http://jvi.asm.org/ on January 4, 2019 by guest

521

522

523

524

525

526

528

529

530

531

532

533

FIG 6. Validation of rLCV circEBNA_U. Upper schematic displays the EBNA U exon and depicts alternative promoters (Cp, Wp, Qp, and Fp) and alternative downstream EBNA coding sequences associated with EBNA U exon containing transcripts. The gel picture shows RNase R resistance of circEBNA_U in all three tumor samples (T1, T2, and T3). cDNAs used in Fig. 3B were used here and the GAPDH PCR shown in Fig. 3b serves as a control for the successful RNase R digestion of linear RNAs.

527

FIG 7. Structure of KSHV circvIRF4 isoforms. A) Graphical presentation of RNase R-seg splicing and coverage data at the vIRF4 locus in latent and TPA treated (reactivation) BCBL1 cells. Backsplicing read counts are represented by the number of under arches, forward splicing is displayed by over arches and exon level coverage data is indicated based on exon color intensity. Single nucleotide resolution coverage data is shown below each splicing graph with amplitudes displayed by negative numbers to represent the leftward orientation of transcription. B) RNase R-resistance and circvIRF4 isoform structure determination. Three different sets of

535

536

537

545

546

547

548

549

550

551

552

553

divergent primer pairs were used with the PP3 primer pair giving rise to two PCR fragments representing a forward spliced (530 bp) and an intron retained (632 bp) version of circvIRF4. Analyses were carried out using naturally KSHV positive BCBL1 cells and in KSHV infected TIVE and iSLK cells.

FIG 8. Detection and validation of lytic MHV68 circM11_ORF69. A) Graphical representation of RNase R-seq 538 539 splicing and coverage data at the ORF69 - M11 locus. Backsplicing read counts are represented by the 540 number of under arches, forward splicing is displayed by over arches and exon level coverage data is indicated 541 based on exon color intensity. Single nucleotide resolution coverage data is shown above the splicing graph 542 with amplitudes representing forward transcription. Primer sites used in panels B and C are indicated. B) 543 Uninfected (-) or infected (MHV68) NIH 3T12 cells 18 hrs after infection were harvested and RNAs were 544 generated. The RNAs were subjected to mock or RNase R treatment and PCR was performed using the

FIG 9. Expression of the rLCV circRPMS1_E5/E5'_E3a EBV homologues, circRPMS1_E4_E2 (upper band) and circRPMS1_E4_E3a (lower band) in primary stomach cancer specimens. N1 and N2 are normal adjacent tissue samples corresponding to the T1 and T2 tumor samples, respectively. Tumor samples, T3 and T5 were assessed previously for circRPMS1_E4_E2 and circRPMS1_E4_E3a and similarly found to be positive (23). SNU719 and YCCEL1 are naturally EBV infected stomach cancer cell lines.

indicated primers. C) RNA isolated from MHV68 infected NIH 3T12 cells, 18 hrs post-infection, were mock or

RNase R treated and PCR was performed using the indicated primers.

Downloaded from http://jvi.asm.org/ on January 4, 2019 by guest

554 **REFERENCES**

- Strong MJ, Laskow T, Nakhoul H, Blanchard E, Liu Y, Wang X, Baddoo M, Lin Z, Yin Q, 555 Flemington EK. 2015. Latency expression of the Epstein-Barr virus-encoded MHC class I TAP 556 557 inhibitor, BNLF2a in EBV-positive gastric carcinomas. J Virol doi:10.1128/JVI.01110-15.
- 558 2. Strong MJ, O'Grady T, Lin Z, Xu G, Baddoo M, Parsons C, Zhang K, Taylor CM, Flemington EK. 559 2013. Epstein-Barr virus and human herpesvirus 6 detection in a non-Hodgkin's diffuse large B-cell 560 lymphoma cohort by using RNA sequencing. J Virol 87:13059-13062.
- 561 3. Strong MJ, Xu G, Coco J, Baribault C, Vinay DS, Lacey MR, Strong AL, Lehman TA, Seddon MB, 562 Lin Z, Concha M, Baddoo M, Ferris M, Swan KF, Sullivan DE, Burow ME, Taylor CM, Flemington 563 EK. 2013. Differences in gastric carcinoma microenvironment stratify according to EBV infection 564 intensity: implications for possible immune adjuvant therapy, PLoS Pathog 9:e1003341.
- Hu L, Lin Z, Wu Y, Dong J, Zhao B, Cheng Y, Huang P, Xu L, Xia T, Xiong D, Wang H, Li M, Guo 565 4. 566 L, Kieff E, Zeng Y, Zhong Q, Zeng M. 2016. Comprehensive profiling of EBV gene expression in 567 nasopharyngeal carcinoma through paired-end transcriptome sequencing. Front Med 10:61-75.
- 568 5. Arvey A, Ojesina Al, Pedamallu CS, Ballon G, Jung J, Duke F, Leoncini L, De Falco G, Bressman 569 E, Tam W, Chadburn A, Meyerson M, Cesarman E. 2015. The tumor virus landscape of AIDS-related 570 lymphomas. Blood 125:e14-22.
- 571 6. Cancer Genome Atlas Research N. 2014. Comprehensive molecular characterization of gastric 572 adenocarcinoma. Nature 513:202-209.
- 573 7. Gottwein E, Corcoran DL, Mukherjee N, Skalsky RL, Hafner M, Nusbaum JD, Shamulailatpam P, 574 Love CL, Dave SS, Tuschl T, Ohler U, Cullen BR. 2011. Viral microRNA targetome of KSHV-infected 575 primary effusion lymphoma cell lines. Cell Host Microbe 10:515-526.
- Skalsky RL, Corcoran DL, Gottwein E, Frank CL, Kang D, Hafner M, Nusbaum JD, Feederle R, 576 8. Delecluse HJ, Luftig MA, Tuschl T, Ohler U, Cullen BR. The viral and cellular microRNA targetome 577 in lymphoblastoid cell lines. PLoS Pathog 8:e1002484. 578
- 9. Pfeffer S, Zavolan M, Grasser FA, Chien M, Russo JJ, Ju J, John B, Enright AJ, Marks D, Sander 579 580 C. Tuschl T. 2004. Identification of virus-encoded microRNAs. Science 304:734-736.
- 10. Cai X, Schafer A, Lu S, Bilello JP, Desrosiers RC, Edwards R, Raab-Traub N, Cullen BR. 2006. 581 Epstein-Barr virus microRNAs are evolutionarily conserved and differentially expressed. PLoS Pathog 582 583
- 11. Chen HL, Lung MM, Sham JS, Choy DT, Griffin BE, Ng MH. 1992. Transcription of BamHI-A region 584 585 of the EBV genome in NPC tissues and B cells. Virology 191:193-201.
- 586 12. Marquitz AR, Mathur A, Edwards RH, Raab-Traub N. 2015. Host Gene Expression Is Regulated by Two Types of Noncoding RNAs Transcribed from the Epstein-Barr Virus BamHI A Rightward Transcript 587 588 Region. J Virol 89:11256-11268.
- 589 13. Howe JG, Steitz JA. 1986. Localization of Epstein-Barr virus-encoded small RNAs by in situ 590 hybridization. Proc Natl Acad Sci U S A 83:9006-9010.
- Lerner MR, Andrews NC, Miller G, Steitz JA. 1981. Two small RNAs encoded by Epstein-Barr virus 591 14. 592 and complexed with protein are precipitated by antibodies from patients with systemic lupus 593 erythematosus. Proc Natl Acad Sci U S A 78:805-809.
- 594 15. Moss WN, Lee N, Pimienta G, Steitz JA. 2014. RNA families in Epstein-Barr virus. RNA Biol 11:10-595
 - 16. Kolakofsky D. 1976. Isolation and characterization of Sendai virus DI-RNAs. Cell 8:547-555.
- 597 17. Hsu MT, Coca-Prados M. 1979. Electron microscopic evidence for the circular form of RNA in the 598 cytoplasm of eukaryotic cells. Nature 280:339-340.
- 599 18. Arnberg AC, Van Ommen GJ, Grivell LA, Van Bruggen EF, Borst P. 1980. Some yeast 600 mitochondrial RNAs are circular. Cell 19:313-319.
- 601 19. Salzman J, Chen RE, Olsen MN, Wang PL, Brown PO. 2013. Cell-type specific features of circular 602 RNA expression. PLoS Genet 9:e1003777.
- 603 20. Salzman J, Gawad C, Wang PL, Lacayo N, Brown PO. 2012. Circular RNAs are the predominant 604 transcript isoform from hundreds of human genes in diverse cell types. PLoS One 7:e30733.
- 605 21. Rybak-Wolf A, Stottmeister C, Glazar P, Jens M, Pino N, Giusti S, Hanan M, Behm M, Bartok O, 606 Ashwal-Fluss R, Herzog M, Schreyer L, Papavasileiou P, Ivanov A, Ohman M, Refojo D, Kadener

- 607 S, Rajewsky N. 2015. Circular RNAs in the Mammalian Brain Are Highly Abundant, Conserved, and 608 Dynamically Expressed. Mol Cell 58:870-885.
- 22. Kristensen LS, Okholm TLH, Veno MT, Kjems J. 2018. Circular RNAs are abundantly expressed and 609 610 upregulated during human epidermal stem cell differentiation. RNA Biol 15:280-291.
- 611 23. Ungerleider N, Concha M, Lin Z, Roberts C, Wang X, Cao S, Baddoo M, Moss WN, Yu Y, Seddon 612 M, Lehman T, Tibbetts S, Renne R, Dong Y, Flemington EK. 2018. The Epstein Barr virus 613 circRNAome. PLoS Pathog 14:e1007206.
- 614 24. Toptan T, Abere B, Nalesnik MA, Swerdlow SH, Ranganathan S, Lee N, Shair KH, Moore PS, 615 Chang Y. 2018. Circular DNA tumor viruses make circular RNAs. Proc Natl Acad Sci U S A 616 doi:10.1073/pnas.1811728115.
- Rivailler P, Jiang H, Cho YG, Quink C, Wang F. 2002. Complete nucleotide sequence of the rhesus 617 25. 618 lymphocryptovirus: genetic validation for an Epstein-Barr virus animal model. J Virol 76:421-426.
- 619 26. Tagawa T, Gao S, Koparde VN, Gonzalez M, Spouge JL, Serquina AP, Lurain K, Ramaswami R, 620 Uldrick TS, Yarchoan R, Ziegelbauer JM. 2018. Discovery of Kaposi's sarcoma herpesvirus-encoded 621 circular RNAs and a human antiviral circular RNA. Proc Natl Acad Sci U S A 622 doi:10.1073/pnas.1816183115.
- 623 27. O'Grady T, Wang X, zu Bentrup KH, Baddoo M, Concha M, Flemington EK. 2016. Global transcript 624 structure resolution of high gene density genomes through multi-platform data integration. Nucleic 625 Acids Research 44.
- 626 28. Memczak S, Jens M, Elefsinioti A, Torti F, Krueger J, Rybak A, Maier L, Mackowiak SD, 627 Gregersen LH, Munschauer M, Loewer A, Ziebold U, Landthaler M, Kocks C, le Noble F, 628 Rajewsky N. 2013. Circular RNAs are a large class of animal RNAs with regulatory potency. Nature 629 **495:**333-338.
- 630 29. Sample J, Brooks L, Sample C, Young L, Rowe M, Gregory C, Rickinson A, Kieff E. 1991. Restricted Epstein-Barr virus protein expression in Burkitt lymphoma is due to a different Epstein-Barr 631 nuclear antigen 1 transcriptional initiation site. Proc Natl Acad Sci U S A 88:6343-6347. 632
- 30. Speck SH, Strominger JL. 1985. Analysis of the transcript encoding the latent Epstein-Barr virus 633 634 nuclear antigen I: a potentially polycistronic message generated by long-range splicing of several exons. Proc Natl Acad Sci U S A 82:8305-8309. 635
- 31. Robinson JT, Thorvaldsdottir H, Winckler W, Guttman M, Lander ES, Getz G, Mesirov JP. 636 Integrative genomics viewer. Nat Biotechnol 29:24-26. 637
- 32. Cunningham C, Barnard S, Blackbourn DJ, Davison AJ. 2003. Transcription mapping of human 638 639 herpesvirus 8 genes encoding viral interferon regulatory factors. J Gen Virol 84:1471-1483.
- 640 33. Russo JJ, Bohenzky RA, Chien MC, Chen J, Yan M, Maddalena D, Parry JP, Peruzzi D, Edelman IS, Chang Y, Moore PS. 1996. Nucleotide sequence of the Kaposi sarcoma-associated herpesvirus 641 642 (HHV8). Proc Natl Acad Sci U S A 93:14862-14867.
- Kanno T, Sato Y, Sata T, Katano H. 2006. Expression of Kaposi's sarcoma-associated herpesvirus-643 34. encoded K10/10.1 protein in tissues and its interaction with poly(A)-binding protein. Virology 352:100-644 645
- 646 35. Katano H, Sato Y, Kurata T, Mori S, Sata T. 2000. Expression and localization of human herpesvirus 647 8-encoded proteins in primary effusion lymphoma, Kaposi's sarcoma, and multicentric Castleman's 648 disease. Virology 269:335-344.
- 649 36. Forrest JC, Speck SH. 2008. Establishment of B-cell lines latently infected with reactivation-competent 650 murine gammaherpesvirus 68 provides evidence for viral alteration of a DNA damage-signaling 651 cascade. J Virol 82:7688-7699.
- 652 37. Adler H, Steer B, Freimuller K, Haas J. 2007. Murine gammaherpesvirus 68 contains two functional 653 lytic origins of replication. J Virol 81:7300-7305.
- 654 38. Deng H, Chu JT, Park NH, Sun R. 2004. Identification of cis sequences required for lytic DNA 655 replication and packaging of murine gammaherpesvirus 68. J Virol 78:9123-9131.
- 656 39. Gong D, Qi J, Arumugaswami V, Sun R, Deng H. 2009. Identification and functional characterization 657 of the left origin of lytic replication of murine gammaherpesvirus 68. Virology 387:285-295.
- 40. Chen YG, Kim MV, Chen X, Batista PJ, Aoyama S, Wilusz JE, Iwasaki A, Chang HY. 2017. 658 Sensing Self and Foreign Circular RNAs by Intron Identity. Mol Cell 67:228-238 e225. 659

661

662

663 664

665

666

667

668

669

670

671

672

673

674

675

676

677

678

679

680

681

682

683

684 685

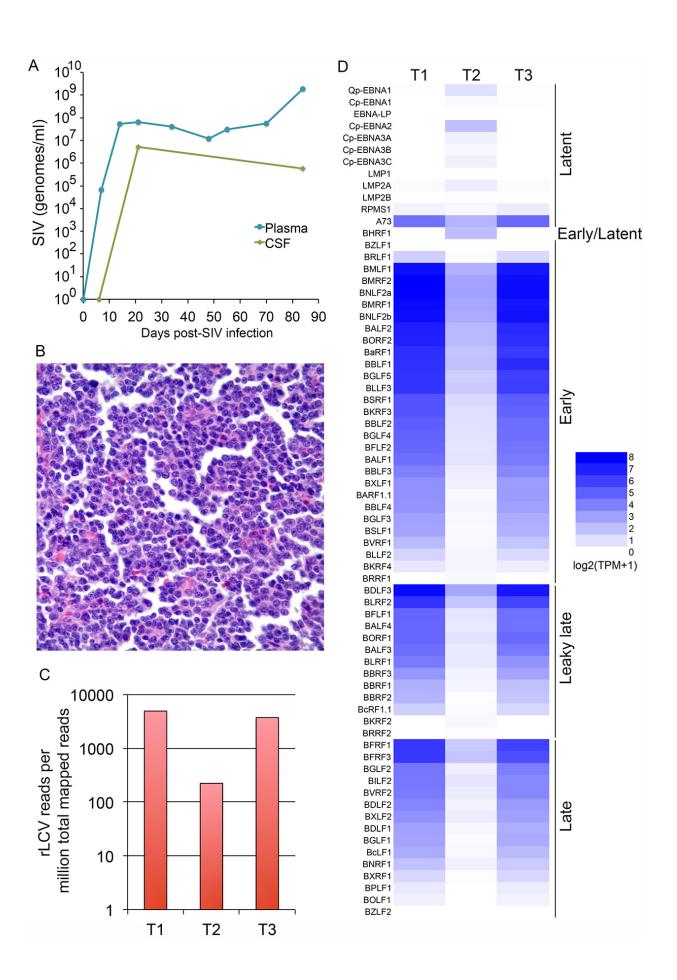
686

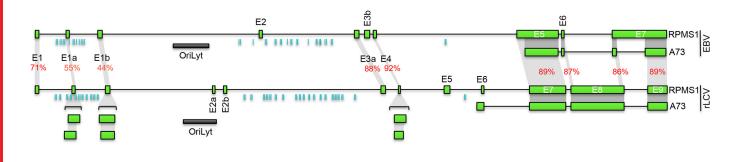
687

688 689

690

- 41. Li X, Liu CX, Xue W, Zhang Y, Jiang S, Yin QF, Wei J, Yao RW, Yang L, Chen LL. 2017. Coordinated circRNA Biogenesis and Function with NF90/NF110 in Viral Infection. Mol Cell 67:214-227
- 42. Singh G, Kucukural A, Cenik C, Leszyk JD, Shaffer SA, Weng Z, Moore MJ. 2012. The cellular EJC interactome reveals higher-order mRNP structure and an EJC-SR protein nexus. Cell 151:750-764.
- Ungerleider N, Maness N, Blair R, Bai S, Roberts C, Moss W, Wang X, Bullard W, Jain V, Surfecz 43. J, Ma T, Dong Y, Renne R, Tibbetts S, Flemington E. 2018. Evolutionary conservation of circRNAs in gammaherpesviruses. J Virol Submitted.
- Hughes DJ, Dickerson CA, Shaner MS, Sample CE, Sample JT. 2011. trans-Repression of protein 44. expression dependent on the Epstein-Barr virus promoter Wp during latency. J Virol 85:11435-11447.
- 45. Rennekamp AJ, Lieberman PM, 2011, Initiation of Epstein-Barr virus lytic replication requires transcription and the formation of a stable RNA-DNA hybrid molecule at OriLyt. J Virol 85:2837-2850.
- 46. Heinzelmann K, Scholz BA, Nowak A, Fossum E, Kremmer E, Haas J, Frank R, Kempkes B. 2010. Kaposi's sarcoma-associated herpesvirus viral interferon regulatory factor 4 (vIRF4/K10) is a novel interaction partner of CSL/CBF1, the major downstream effector of Notch signaling. J Virol 84:12255-12264.
- 47. Xi X, Persson LM, O'Brien MW, Mohr I, Wilson AC. 2012. Cooperation between viral interferon regulatory factor 4 and RTA to activate a subset of Kaposi's sarcoma-associated herpesvirus lytic promoters. J Virol 86:1021-1033.
- 48. Rezaee SA, Cunningham C, Davison AJ, Blackbourn DJ, 2006, Kaposi's sarcoma-associated herpesvirus immune modulation; an overview. J Gen Virol 87:1781-1804.
- 49. Virgin HWt, Latreille P, Wamsley P, Hallsworth K, Weck KE, Dal Canto AJ, Speck SH. 1997. Complete sequence and genomic analysis of murine gammaherpesyirus 68. J Virol 71:5894-5904.
- Dobin A, Davis CA, Schlesinger F, Drenkow J, Zaleski C, Jha S, Batut P, Chaisson M, Gingeras 50. TR. 2013. STAR: ultrafast universal RNA-seg aligner. Bioinformatics 29:15-21.
- 51. Djavadian R, Hayes M, Johannsen E. 2018. CAGE-seg analysis of Epstein-Barr virus lytic gene transcription: 3 kinetic classes from 2 mechanisms. PLoS Pathog 14:e1007114.
- 52. Skalsky RL, Kang D, Linnstaedt SD, Cullen BR. 2014. Evolutionary conservation of primate lymphocryptovirus microRNA targets. J Virol 88:1617-1635.





			Coordinates			
£ 12	0		(rLCV_inverted)	T1	T2	T3
100 50	0	circRPMS1_E5'_E3a	43548-46167			
	ס	circRPMS1_E5_E3a	43548-46173			
Read	5	circRPMS1_E2b'_E1b	32964-37563			
<u>س</u> ۱	כ	circRPMS1_E2b_E1b	32964-37584			
		circEBNA_U	118000-118171			

E5' E5 GTACAC

...ACCCCGCCCAG GTAGAG GTACAC

E2b' E2b E2b GTATTGCTTCTATTCTTGAAC GTGAGA

Downloaded from http://jvi.asm.org/ on January 4, 2019 by guest

